POLITECNICO DI TORINO
Repository ISTITUZIONALE

Potential of double pilot injection strategies optimized with the design of experiments procedure to improve diesel engine emissions and performance

(Article begins on next page)

02 May 2024

POTENTIAL OF DOUBLE PILOT INJECTION STRATEGIES OPTIMIZED WITH A DESIGN OF EXPERIMENTS PROCEDURE TO IMPROVE DIESEL ENGINE EMISSIONS AND PERFORMANCE.

d'Ambrosio, S. , and Ferrari, A.[*]

Energy Department – Politecnico di Torino

C.so duca degli Abruzzi, 24, 10129, Torino, Italy.

ABSTRACT

The potential of pilot-pilot-main triple injection strategies versus engine out emissions, combustion noise and brake specific fuel consumption has been assessed experimentally on a Euro 5 diesel engine with a reduced compression ratio (16.3:1). The engine has been fueled with conventional diesel fuel. The experimental tests on the engine have been carried out in a dynamometer cell under different steady state working conditions, that are representative of passenger car engine applications over the European homologation cycle. Furthermore, in-cylinder analyses of the pressure, heat-release rate, temperature and emissions have been performed in order to obtain more detailed knowledge on the cause-and-effect-relationships between the implemented injection strategies and the results of the experimental tests.

The implemented double-pilot injection engine calibrations have been optimized by means of the design of experiments procedure. The plotted data of the engine performance and emissions have been compared with data from the original double-injection schedule, characterized by a retarded main injection timing, in order to intensify the premixed combustion phase. The benefits and the disadvantages of the *PCCI* concept are preliminarily discussed, on the basis of the experimental pilot-main injection strategy results.

The substitution of the pilot-main injection schedule with the triple injection, for light engine loads and low engine speeds, has led to higher combustion pressures, lower heat release rates, shorter ignition delays and lower brake specific fuel consumption. Above all, a significant improvement in engine noise and in both *CO* and *HC* engine-out emissions has been achieved and the NO_x emission have been limited by the application of high *EGR* rates. When medium engine loads and speeds are analyzed, the considered double-pilot injection strategy allows the NO_x emissions to be reduced, compared to the baseline pilot-main injection schedule. However, the combustion noise does not improve and the soot deteriorates, even though the soot penalties are not relevant.

[*] Corresponding author e-mail address: alessandro.ferrari@polito.it.

28   **Highlights:**

29   -   The benefits and the weak points of the partial *PCCI* strategy for low loads and speeds are discussed.

30   -   The effects of the triple pilot-pilot-main injection on engine-out emissions and noise are analyzed.

31   -   The experimental tests on the multiple injections are supported by numerical in-cylinder analyses.

1.   INTRODUCTION

33   The implementation of a pilot injection in diesel engines makes the entire amount of the fuel chemical energy be

34   released over a prolonged time interval, thus determining a longer combustion than for the single injection case.

35   Furthermore, the premixed combustion of some of the pilot injected fuel causes a slight increase in the in-cylinder gas

36   pressure and temperature [1] before the main injection has occurred, and therefore leads to a considerable reduction in

37   the ignition delay of the main injection [2]. This reduction in the fuel ignition delay limits the impact of the premixed

38   combustion and generates a less rapid heat release rate [3] during the main injection than in a single injection schedule

39   [4]. As a consequence, the main combustion becomes predominantly mixing-controlled [3].

40   A pilot injection that is sufficiently close to the main injection has the potential of enhancing combustion efficiency and

41   thus brake specific fuel consumption (*bsfc*), because the pilot and main combustions are linked smoothly [5]. Pilot

42   injections are also effective in decreasing combustion noise (*CN*), especially at engine idle [3]. Reductions of up to 5-8

43   dB are generally obtained in the *CN*, compared to single injection strategies [6-8].

44   Since the pilot injection decreases the impact of the overall premixed combustion, it makes the highest flame

45   temperatures diminish and, as a consequence, the NO_x emissions generally also reduce, compared to the single-injection

46   strategy [9]. However, large pilot injected quantities make the NO_x produced in the pilot combustion grow, and the

47   increase in the NO_x amount produced by the pilot combustion can surpass the decrease in the main combustion NO_x

48   emissions, due to the shortened ignition delay [10]. Furthermore, when heavy *EGR* rates (~60%) are employed, such as

49   in partial *PCCI* strategies, the pilot injection timing and mass do not influence the NO_x emissions to any appreciable

50   extent because the NO_x emissions are very small [5].

51   The smoke emission in pilot-main injections generally tends to increase, compared to single injections. In fact, the pilot

52   injection increases the in-cylinder temperature and decreases the oxygen concentration in the gases before the main

53   injection has occurred. Both of these effects generally make the smoke emission grow: the increased temperature

54   mainly acts by reducing the lift-off length, which pertains to the main injection, with a subsequent increase in the

55   equivalence ratios close to the nozzle. The insufficient mixing of fuel with air, which is also due to the shortened

ignition delay of the main injection, augments the percentage of the diffusion combustion in the main combustion and, as a consequence, the final soot level grows [11]. In general, the quantity of the pilot injection should be below a certain threshold (a general value of 4 mg is normal) in order to contain the smoke number [12].

Finally, HC and CO emissions reduce at low loads if a pilot injection is implemented, because the occurrence of overmixing is ~~more~~ less likely. In particular, the CO conversion rate improves because of the relatively high in-cylinder temperature and the shorter ignition delay of the fuel injected in the main injection [4].

The pilot injection can be exploited in different ways to improve engine-out emissions, CN and fuel consumption, depending on the working condition [13]. Soot emissions are not relevant at low engine speeds and loads, NO_x and noise are usually controlled, at these conditions, by means of adequate EGR rates. The pilot injection is generally optimized, on the basis of the EGR rate, in order to reduce HC and CO emissions [14], which tend to be high, due to the presence of lean and cool regions. The HC and CO emission situation becomes worse at engine cold start and warm-up, when the oxidation catalyst has less conversion efficiency. Soot, NO_x, noise and $bsfc$ are the dominant problems at medium load conditions, that is, in the higher load zone of the $NEDC$ region, whereas HC and CO are not of great concern. Pilot injections are therefore used in these conditions to improve PM-NO_x and $bsfc$-NO_x trade-offs and, above all, CN [15].

Pilot injection is generally applied to the $NEDC$ area, but it can also be used for other purposes and offers other benefits. An early pilot injection can be applied to increase the in-cylinder pressure at the end of the compression stroke during engine cranking, thus reducing the engine start time. Furthermore, pilot-main injection patterns reduce the cycle-to-cycle variability of the torque, compared to single injections [4], and this induces more stable engine operation, especially after the engine crank phase [16]. Finally, pilot injection can be used at full load to limit the peak in-cylinder pressure and the engine exhaust temperature. The noise due to combustion is less important at these engine working conditions, since other sources of noise dominate in the vehicle, and the pilot injection therefore allows either the fuel rate to be increased or the mechanical and thermal stresses in the engine to be reduced, thus providing possible weight savings or simplifications of the cooling circuit. Instead, when the maximum torque is smoke limited, an early pilot injection can increase the full load torque by improving the utilization of the air within the cylinder, compared to the case of a single injection with a long energizing time [17]. In general, the pilot injection shot can also be used at high loads to reduce soot and improve combustion efficiency, since the main injection duration can be shortened.

The fundamental pilot-main injection scheme constitutes the conceptual basis for the development of more sophisticated and advanced multiple injection strategies that can implement multiple pilot injection shots. Pilot-pilot-main injection schedules have been shown to have a great potential toward noise [18, 19], emission [20, 21] and $bsfc$ [20, 22, 19] reductions. However, more trials are required to optimize various engine parameters, such as the EGR rate,

87   the swirl actuator position, the boost pressure, the dwell-time, the injection timings, the rail pressure and the energizing

88   times of all of the injection shots, and thus to be able to fully exploit these strategies [23]. In the present work, a design

89   of experiment *(DoE)* procedure has been applied to optimize the double-pilot injection engine calibration. This

90   innovative approach allows the effective benefits of this injection strategy to be assessed, since optimized pilot-pilot-

91   main and pilot-main injection engine calibrations are compared. In general, the aims of the double-pilot injection

92   strategy should be selected on the basis of the engine working conditions and the installed aftertreatment devices. The

93   triple injection in the current investigation is principally aimed at minimizing NO_x and combustion noise. Furthermore,

94   the double- and triple-injection strategies are tested under high *EGR* conditions, whereas most of the research on

95   multiple injections has been conducted under low or moderate *EGR* rates (moderate *EGR* rates correspond to EGR

96   fractions up to 30-40%) [24].

2.   EXPERIMENTAL FACILITIES AND ENGINE SETUP.

98   The experimental tests have been carried out on the dynamic test bed installed at the Politecnico di Torino *IC*

99   laboratories. The test rig is equipped with an '*ELIN AVL APA* 100' cradle-mounted *AC* dynamometer, featuring

100   nominal torque and power of 525 Nm and 220 kW, respectively, as well as a maximum speed of 12000 rpm. The

101   facility is capable of full four-quadrant operation with high speed and torque dynamics, as well as the simulation of zero

102   torque and gear shifting oscillations in the drivetrain.

103   The test facility is equipped with a '*Pierburg AVL AMA 4000*' raw exhaust-gas analyzer, which is basically made up of

104   three analyzer trains. Two of these trains feature the following modules: one heated flame ionization detector for the

105   *THC* analysis, one heated chemiluminescence detector for the analysis of the NO_x, three nondispersive infrared

106   analyzers for the measuring of low as well as high *CO* and CO_2 concentration levels and one paramagnetic oxygen

107   detector for the O_2 levels. These two trains allow the pollutant emissions to be measured simultaneously, upstream and

108   downstream of the aftertreatment system. The third train is made up of a CO_2 concentration detector for the measuring

109   of the CO_2 concentrations in the inlet manifold, in order to be able to calculate the *EGR* mass fraction, which is defined

110   as $X_{EGR} = \dot{m}_{EGR}/(\dot{m}_{EGR} + \dot{m}_a)$, according to the procedure developed in [25].

111   As far as the particulate matter (*PM*) measurement is concerned, the dynamic test bed is equipped with the following

112   instruments: *AVL 415S* smokemeter, *AVL 439S* opacimeter and *AVL SPC472* Smart Sampler. Finally, an '*AVL KMA*

113   *4000 Methanol*' measuring system continuously meters the engine fuel consumption. This system is based on the *AVL*

114   *PLU* measuring principle of a servo-controlled positive displacement counter, and it can perform measurements over

115   the 0.28-110 kg/h range with a reading accuracy of 0.1% for diesel fuel.

116 All of the abovementioned measurement devices are controlled by a *PUMA OPEN 1.3.2* automation system, which also

117 includes *ISAC 400* software for the simulation of the behavior of both the vehicle (road load, road gradient and

118 moments of inertia of the driveline components, which are not physically present on the test bed) and of the driver

119 behavior (use of the clutch, accelerator pedal and gear shifting).

120 The tested engine, the main features of which are reported in Table 1, is a Euro 5 engine fueled with conventional diesel

121 oil. It has been fully instrumented with piezoresistive pressure transducers and thermocouples for the measurement of

122 the pressure and temperature levels at the following locations: upstream and downstream of the compressor, at the inlet

123 manifold, upstream and downstream of the turbine and downstream of the aftertreatment system. Additional

124 thermocouples have also been installed for the measurement of the temperatures downstream of the intercooler, in the

125 four inlet and exhaust runners, as well as upstream and downstream of the *EGR* cooler. Finally, an *UEGO* air-fuel ratio

126 sensor has been located within the exhaust system. The acquisition of all of these time-averaged quantities are directly

127 managed directly by the *PUMA OPEN 1.3.2* system, through a dedicated firewire front-end module, which can manage

128 up to 48 analog input channels with a maximum data capture rate of 5 kHz per channel.

129 A high-frequency piezoelectric transducer has been installed on the engine cylinder head to measure the pressure time-

130 history of the gases in one of the cylinders, whereas another high-frequency piezoresistive transducer has been used to

131 detect the pressure levels in the inlet runner of the same cylinder in order to reference the in-cylinder pressure. An *AVL*

132 *365C* crank-shaft driven encoder generates the time base for an automatic 14 bit data-acquisition system (based on the

133 *AVL* indimodul 620 system), which is capable of acquiring up to 8 channel data with a maximum frequency of 800 kHz

134 per channel. The acquisition system is managed by *AVL Indicom* software, in order to allow both the online analysis of

135 the indicated cycle and data storage operation for post-processing with a validated three-zone combustion diagnostic

136 tool [26]. In this model, the combustion chamber content is divided into three zones: a fuel zone, an unburned gas zone,

137 (containing fresh-air, residual gas and *EGR*) and a burned gas zone obtained from a global stoichiometric combustion

138 process. Ordinary differential mass and energy conservation equations are applied to the three zones and are solved

139 numerically on the basis of the experimental in-cylinder pressure. The model allows the temperatures of the three zones

140 to be predicted as functions of the crank angle. Furthermore, thermal and prompt NO mechanisms are implemented in

141 the code, according to the Zeldovich and Fenimore submodels, respectively. The soot formation is modeled [27] by

142 means of an expression that uses the mean air-fuel ratio over the combustion interval, whereas the soot oxidation rate is

143 modeled using an empirical formula, based on the temperature of the burned gas zone.

3. THE DESIGN OF THE EXPERIMENT PROCEDURE

The tested engine was calibrated by the *OEM* with a double injection strategy, which represented the state-of-the-art pilot-main injection schedule for the considered engine technology.

The *ppM* injection strategies have been optimized by adopting the statistical design of the experiments (*DoE*) technique.

The following parameters were considered as the most relevant input variables for the procedure: rail pressure (p_{Rail}), swirl actuator position (*Sw*), dwell times (*DT*) between consecutive injections (DT_2 between the pilot 2 and pilot 1 shots and DT_1 between the pilot 1 and main shots, where pilot 1 is the closest shot to the main injection and pilot 2 the furthest shot from the main injection), main injection timing (SOI_{Main}), the injection quantities in each shot (q_{Pil1} and q_{Pil2}) and the inducted air per stroke and per cylinder (m_a).

Key-points are engine working points (characterized in terms of *bmep* [bar] and speed *n* [rpm]), considered as representative of the engine application to a passenger car over the new European driving cycle. The following key-points were considered for the tested engine ($n \times bmep$): 1500×2, 1500×5, 2000×2, 2000×5, 2500×8, 2750×12 and idle.

Tables 2 and 3 report (second column) the parameter levels that were considered in the variation lists for the optimization of the *ppM* injection schedule at the 1500×2 and 2000×5 key-points. The center and the extreme values of the range that were considered for each parameter were chosen on the basis of preliminary measurements. An appropriate number of levels was selected in order to obtain accurate results with a reasonable number of tests for each variation list. The quantity of fuel in the main injection is set by the test-bench control system in order to guarantee the *bmep* value, and is therefore not present as a parameter in the variation list. The *EGR* ratio affects the emissions at the diesel engine exhaust to a great extent. However, the *ECU* does not evaluate this parameter directly, but can measure m_a (by means of the air mass flowmeter), which is intimately connected to *EGR*. Therefore, the information related to the induced air, m_a, was considered in the variation lists, instead of the *EGR* ratio.

The preliminary variation list was obtained using the Matlab Model-Based Calibration toolbox, setting a V-optimal type design of experiments, which minimizes the prediction error variance, and a full factorial series, as the candidate set, on the basis of the levels shown in Tables 2 and 3. The preliminary variation list was then randomized and replications of the central point (defined by the center value of each parameter range) were added every 10-15 points in order to further reduce the prediction error variance and check for any possible drifts of the output variables for fixed input parameters. The final variation lists were made up of 120-150 tests for each considered key-point. Once the variation list tests had been carried, it was possible to obtain quadratic models of the output variables as functions of the input variables and of their interactions.

The engine-out specific NO_x, *CO*, *HC* and soot emissions, the *bsfc* and the *CN* were considered as the output variables. Different targets can be introduced for the output variables in order to select the best set of values for the input variables

175 at each key point, that is, the optimized engine calibration. The optimization procedure consists of a number of

176 constraints on the output variables. These constraints depend on the pollutant emission regulations, on the aftertreatment

177 devices that are installed on the engine, on the CO_2 targets and on aspects related to fun to-drive.

178 The considered Euro 5 engine was equipped with a diesel oxygen catalyst (*DOC*) and a particulate filter, but no

179 aftertreatment device was designed to reduce the NO_x emissions. The optimization strategy for the triple (pilot-pilot-

180 main) injection schedules, based on the *DoE*, was aimed at minimizing NO_x emissions and at reducing the combustion

181 noise with respect to the pilot-main injection calibration, which was originally implemented in the ECU provided by the

182 engine *OEM*. However, rather severe upper limits were also set for *CO*, *HC* and *bsfc*.

183 Tables 4 and 5 show the reference values of the output variables for the pilot-main injection strategy and the constraints

184 used for the optimization of the triple injection strategy. The optimum values of the input variables, calculated by means

185 if the *DoE* procedure, are reported in the third column of Tables 2 and 3. *EGR* trade-offs were performed in the

186 neighborhood of the calibration baseline points for both the double and the optimized triple injection strategies in order

187 to compare not only the baseline points of the two calibrations, but also two complete curves.

4.   LIGHT LOAD CONDITIONS.

4.1   PCCI-like double-injection strategies

190 Figures 1-3 report the in-cylinder pressure (p_{cyl}), the heat release rate (*HRR*) and the burned gas temperature (T_b) time

191 histories, respectively, for n = 1500 rpm and *bmep*=2 bar. The continuous curves with square- and circle-symbols refer

192 to $X_{EGR} \approx 50\%$ and $X_{EGR} \approx 28\%$, respectively (these two operating conditions correspond to high and moderate *EGR* rates),

193 and the same pilot-main (*pM*) strategy is adopted in both cases. Since the injection strategy is the same, these

194 preliminary tests are aimed at assessing the effect of the *EGR* rate in *PCCI* engines. The p_{cyl} trace has been measured by

195 means of the piezoresistive pressure transducer installed in the combustion chamber, while the *HRR*, and the T_b time

196 histories have been calculated by means of the three-zone combustion diagnostic tool.

197 A relatively high dwell time between the pilot and the main injection ($DT \approx 1400$ μs) has been implemented (cf. Fig. 2)

198 and a vigorous swirl has been applied to promote the air-to-fuel mixing. The heavy *EGR* rate condition that corresponds

199 to $X_{EGR} \approx 50\%$ has been applied in order to prolong the fuel ignition delay and obtain a partially homogeneous mixture

200 before ignition [28]. Fig.1 shows that the in-cylinder pressure decreases as the *EGR* is increased. In fact, both the flow-

201 rate through the turbine and the upstream pressure are reduced when high *EGR* rates are applied to a short-route *EGR*

202 system (cf. also the schematic of the engine in Table 1). As a consequence, the system may not be able to maintain the

203 desired boost level and a decrease in the boost may therefore be experienced at high *EGR* rates, especially for low

204   loads. The decrease in the in-cylinder pressure with increasing *EGR* in Fig. 1 is due to the reduction in the boost

205   pressure and to the increase in the temperature of the cooled *EGR*, compared to the temperature of the fresh air coming

206   from the engine intercooler. Figs. 2 and 3 show that high fractions of cooled *EGR* and retarded main injection timings

207   allow the maximum *HRR* and the T_b peak value to be contained [29], and the ignition delay of both the pilot and main

208   injected fuel to be lengthened, compared to the moderate *EGR* rate condition ($X_{EGR} \approx 28\%$). In particular, it can be

209   observed that the pilot combustion in the $X_{EGR} \approx 50\%$ case exhibits a two-stage ignition with the presence of both cool

210   and hot flame reactions, whereas single-stage pilot combustion occurs at $X_{EGR} \approx 28\%$.

211   The considered pilot-main (*pM*) injection schedule realizes a highly premixed combustion concept, since the main

212   combustion event starts when the main injection has finished. Most of the fuel injected during the pilot and the main

213   shots burns in premixed combustion conditions. The *HRR* peak, related to the diffusive combustion of the main injected

214   fuel, can be seen in Fig. 2 for $X_{EGR} \approx 28\%$, but vanishes for $X_{EGR} \approx 50\%$. The advantage of the implemented strategy is that

215   it induces a simultaneous reduction in soot and NO_x emissions, due to the intensified fuel premixing and to the reduced

216   combustion temperature. Fig. 4 shows that both the soot and NO_x emissions decrease when the *EGR* rate is increased

217   progressively, while the other engine parameters remain constant (the contoured triangle symbol represents the *EGR*

218   rate of the baseline pilot-main injection calibration); this behavior, with respect to X_{EGR}, is not observed when more

219   conventional double-injection patterns are applied. Fig. 5 shows the gas temperature at the diesel oxygen catalytic

220   catalyst inlet (T_{cat}) as a function of the *EGR* rate. The experimental points, evaluated as functions of NO_x in Fig 4 and as

221   functions of *EGR* rate in Fig.5, are the same (maximum NO_x corresponds to minimum X_{EGR} and vice versa).

222   Higher X_{EGR} levels than 50% are in line with partial *PCCI* applications, which intensify the local mixing of the fuel

223   plume and the charge, with the production of a premixed stratified charge. Furthermore, the selected engine

224   compression ratio was $\varepsilon = 16.3$, which falls between the typical values of conventional diesel engines ($\varepsilon = 17 \div 18$) and the

225   characteristic values of partial *PCCI* engines ($\varepsilon = 13 \div 16$, [30]). The reduced compression ratio makes the temperature

226   and pressure, which are closely related to NO_x formation, decrease during the compression phase. This enables the fuel

227   spray to penetrate further with more air entrainment, thus contributing to a decrease in the soot [31], which is also due

228   to the increase in the fuel autoignition delay [32, 33]. Finally, a toroidal combustion-bowl was selected, in line with

229   partial *PCCI* applications, since it assures a rapid fuel mixing when combined with a high swirl number, and a large

230   bowl piston diameter was designed in order to reduce the occurrence of wall impingement. However, unlike typical

231   partial *PCCI* combustion diagrams, the pilot injected fuel does not burn together with the main injected fuel, and a pilot

232   combustion event, which is not connected to the main combustion, can be observed in the *HRR* traces reported in Fig. 2.

233   Furthermore, the ratio of the quantity injected in the main shot to that injected in the pilot shot is significantly higher

234   than that usually adopted in partial *PCCI* engines.

235   Pilot injection quantities with early injection timings, like the typical ones used in early *PCCI* injection strategies (40-50

236   *BTDC* degrees), can cause the fuel vapor to spread to the cylinder liner, because the in-cylinder charge pressure and

237   density are low for early injection timings and light loads. This leads to overmixed regions and wall quenching

238   phenomena, both of which are important sources of *HC* and *CO* emissions. In addition, the possible spray impingement

239   on the wall surfaces dramatically increases the amount of unburned hydrocarbons [34], dilutes the lubrication oil and

240   causes the fuel consumption to increase to a great extent, since part of the pilot injected fuel is wasted and unable to

241   ignite. For these reasons, the relatively long dwell time in the pilot-main injection pattern, which is reported in Fig. 2,

242   has been introduced by further delaying the main injection rather than by advancing the pilot injection. Since the pilot

243   injection does not occur very early during the piston compression stroke, and the pilot injected quantity is contained

244   ($V_{pil} \approx 1.7$ mm^3), wall impingement occurrence is not a concern. Furthermore, the retarded main combustion contributes

245   to the generation of a reduced soot formation rate because the peak in-cylinder temperature around *TDC* is contained

246   and an enhanced soot oxidation rate can be observed during expansion and blowdown phases, due to the raised burned

247   gas temperatures during the last part of the expansion stroke and at the engine exhaust.

248   The considered *pM* injection pattern features high levels of *HC* and *CO* emissions, due to low-temperature combustion

249   [35] and fuel overmixing, as well as elevated combustion noise, due to the highly premixed combustion. Furthermore,

250   the *bsfc* become worse, compared to the double injection strategies implemented in conventional diesel engines, due to

251   the retarded main injection timing (SOI_{Main}) and the diminished ε value. These drawbacks are of the same typology as

252   those encountered in classic partial *PCCI* engines featuring late injection strategies.

253   A minimum temperature level of 200°C is necessary at the catalytic converter inlet (T_{cat}) to obtain a satisfactory

254   efficiency of the diesel oxygen catalyst (*DOC*) for the conversion of the high *HC* and *CO* engine-out emissions at low

255   loads. The T_{cat} values in Fig. 5 can be seen to be higher than this threshold for $X_{EGR} > 45\%$.

256   Since the main injected quantity is much larger than the pilot injected mass, the SOI_{Main}, which is equal to 1° *CA ADTC*

257   in Fig. 2, has not been delayed any further, as occurs in typical late *PCCI* injection strategies, in order to avoid an

258   excessive *bsfc* penalty. In fact, the SOI_{Main} varies within the 3-10° *CA ATDC* range for late *PCCI* injection strategies,

259   whereas it is usually in the 5-7° *CA BTDC* range for diesel engines with conventional combustion systems.

260   **4.2   Triple injection strategies.**

261   Figures 6-8 show comparisons of *HC-NO$_x$*, *CO-NO$_x$* and *bsfc-NO$_x$ EGR* trade-off curves obtained for two different

262   engine calibrations in the 45% < X_{EGR} < 55% range and at n = 1500 rpm and *bmep*=2 bar. Fig. 9 instead plots the *NO$_x$*-

263   X_{EGR} curves for the two strategies. The triangle symbols in Figs. 6-9 pertain to the previously discussed *pM* injection

264   engine calibration, whereas the circle symbols refer to a pilot-pilot-main (*ppM*) injection engine calibration. The

265   contoured line symbols correspond to the baseline calibration points of the two strategies. The triple injection baseline

266   calibration has been obtained with the *DoE* campaign; not only has a pilot shot been added to the injection train of the

267   baseline point of the *pM* calibration, but the rail pressure, injection timings, energizing times and other engine

268   parameters have also been changed. The *SOI* of the pilot 1 and pilot 2 injections are in the $10 \div 20$ cad *BTDC* range for

269   the *ppM* strategy, and are in line with the literature results concerning the best pilot injection timings in triple injections

270   [4].

271   It can be observed, from Figs. 6-9, that the *DoE* optimized *ppM* strategy generally allows the *CO* and *HC* emissions to

272   be improved at the same NO_x, with respect to the baseline double injection strategy. Furthermore, a slight enhancement

273   can be detected for the *bsfc-NO_x* trade-off. If reference is made to the calibration baseline points, the NO_x engine-out

274   emissions reduce in the *ppM* case (Fig. 9), in line with [36]. However, the NO_x-X_{EGR} curve is virtually the same for the

275   two strategies and the effectiveness of the *EGR* on the engine-out NO_x emissions therefore does not change for either of

276   the two calibrations.

277   The *ppM* pattern should lead to a decrease in the local air-to-fuel ratio, with respect to time and space, due to the lower

278   global oxygen concentration ($[O_2]_{int}$ =14.9 versus $[O_2]_{int}$=16.0 of the *pM* calibration). The generation of a suitable fuel

279   vapor stratification close to the nozzle reduces the impact of fuel overmixing and wall quenching, and thus decreases

280   the engine out *HC* and *CO* emissions (cf. Figs. 6 and 7). In other words, the pre-combustion, which is due to the

281   introduction of the pilot 1 injection prior to the main injection, plays a role in attaining a sufficient main combustion

282   ignition and in improving the conversion efficiency of the fuel, and thus in enhancing the complete combustion of the

283   main injection. The improvements obtained for the *bsfc-*, *HC-* and *CO-NO_x* tradeoffs, by means of the pilot-pilot-main

284   injection, are in line with the results found in [19-22] for low loads and speeds. In particular, when *EGR* rates close to

285   50% are applied, two pilot injections are recommended [15] in order to decrease the *HC* emissions.

286   The p_{cyl} and the *HRR* curves that refer to the calibration baseline points of both the *pM* and the *ppM* strategies are

287   reported in Figs. 10 and 11, respectively. The *pM* curves have been plotted with solid line and triangle symbols,

288   whereas the *ppM* solid line curves are marked with circle symbols. The two-stage autoignition delay of the pilot 2

289   injection increases for the *ppM* strategy because the pilot 2 injection takes place earlier in the compression stroke, where

290   the charge pressure and temperature are lower. Furthermore, the maximum p_{cyl} value pertaining to the main injection

291   increases when passing from the *pM* to the *ppM* injection schedule, but the *HHR* pilot peaks and the *HRR* main

292   combustion peak reduce when pilot 1 injection is applied because of the decrease in the premixed combustion portion.

293   This evidence on p_{cyl} and *HRR* proves that the combustion performance has improved, and the p_{cyl} and *HRR* trends with

294   the number of injections can be confirmed from those obtained passing from a single injection to one-pilot injection. As

295   can be seen in Fig. 12, the decrease in the maximum *HRR* and the earlier main combustion induce a slight diminution in

296 temperature T_b of the burned gases for $\theta \geq 370°CA$ in the case of the ppM strategy. On the other hand, the earlier SOI_{pil2}

297 of the ppM strategy advances the time instant at which the burned gas temperature jumps to high levels and, as a

298 consequence, the residence time in which the burned gases are exposed to higher temperatures than 1900 K increases

299 for the triple injection calibration. The NO_x formation rates are very sensitive to flame temperatures above 1900-2000 K

300 [37], but, on the basis of the Kamimoto-Bae diagram, NO_x emissions are only produced for smaller local equivalence

301 ratios (ϕ) than 1.5 [38]. A larger amount of mixture with relatively high ϕ values should be obtained in the fuel spray for

302 the ppM strategy, because of the reduced mixing with air and, consequently, the NO_x emissions can reduce. It is the

303 contribution of the main combustion that makes the final levels of NO_x higher for the pM injection schedule (cf. Fig.

304 13).

305 When the two pilot shots are applied, the HRR curve (Fig. 11) remains uninterruptedly higher than zero from the start of

306 the cool flames pertaining to the first pilot injection till the end of the main injected fuel combustion. Fig. 14 shows the

307 crankshaft angle ($MFB50$) that corresponds to a fuel mass burned fraction equal to x_b=0.5, and the diagrams plotted in

308 Figs. 11 and 14 justify the slight $bsfc$ improvement, which in Fig. 8 generally results from the application of the ppM

309 strategy. In fact, the combustion heat is released closer to the TDC in the ppM case than in the pM one, in part due to the

310 more advanced SOI_{Main}.

311 The fuel for the ppM strategy burns with a more regular combustion rate, as can be seen in Fig.11 and without high-time

312 derivatives in the burned gas mass fraction time history (cf. also Fig. 14). As a consequence, a remarkable decrease in

313 the combustion noise can be expected, and the CN-NO_x curve in Fig. 15 in fact improves significantly for the triple

314 injection strategy, compared to the pM injection schedule (reductions of up to 3.5 dB can occur). This is a consequence

315 of the decrease in the dwell times between the consecutive injection shots, compared to the pM case. In fact, the

316 reduction in the premixed combustion portion for the ppM strategy makes combustion noise decrease. The advanced

317 SOI_{Main} in the ppM injection pattern was purposely implemented in order to reduce the combustion noise. The mass

318 fraction of burned fuel, before the start of the main injection in Fig. 14, is equal to 15% and to 12% for the pM and the

319 ppM strategies, respectively, while the minimum noise condition generally corresponds to approximately 8% [8].

320 Figures 16 and 17 show the combustion noise Fourier spectra, evaluated at n=1500 rpm and $bmep$=2 bar, for the pM and

321 the ppM strategies, respectively. The solid bars in each figure refer to the $X_{EGR} \approx 49 \div 50\%$ case, whereas the hatched bars

322 refer to $X_{EGR} \approx 52 \div 53\%$. A frequency range (500$\div$2000 Hz), in which the spectral combustion noise takes on the highest

323 values, exists in each Fourier spectrum. The presence of a pronounced peak zone, which occurs within a narrow

324 frequency band, is more evident for the pM diagram at $X_{EGR} \approx 49 \div 50\%$, even though the peak zone tends to disappear as

325 the value of X_{EGR} is increased. The presence of a peak zone in the diagrams in Figs. 16 and 17 indicates that there is an

326 overly dominant frequency range in the signal, which gives tonality to the noise. In other words, the higher the peak

327   intensity and the smaller the extension of the peak zone, the more recognizable the combustion noise as a specific noise.

328   The sensitivity of the combustion noise to *EGR* variations is limited for the *ppM* strategy, while the tonality is more

329   reduced for the *pM* pattern as the *EGR* passes from $X_{EGR} \approx 50\%$ to $X_{EGR} \approx 53\%$. Since the human ear is very sensitive to

330   changes in noise, a triple injection can contribute to a less irritating perception of the combustion noise when the *EGR*

331   rate is modified.

332   Finally, the increase in soot emissions, which can be observable in Figs. 18 and 19 for the triple injection, is not of real

333   concern since the smoke emissions continue to show relatively low values (Soot<0.31 g/kWh in Fig. 18 and Soot<0.01

334   mg in Fig. 19), due to the low peak in-cylinder temperatures and the high relative air-to-fuel ratio (λ) for these engine

335   working conditions. The presence of a soot-NO_x trade-off curve, in the case of the *ppM* injection strategy, shows that

336   the combustion does not feature *PCCI*-like behavior, unlike the *pM* case.

337   All of the previous explanations and conclusions about the effects that the addition of a second pilot injection has on

338   engine emissions, combustion noise and *bsfc* performance have been based on experimental data at *n*=1500 rpm and

339   *bmep*=2 bar, but they can be extended to the whole area for light loads, from low to medium engine speeds. This can be

340   confirmed from the experimental results plotted in Figs. 20-24, which refer to *n*=2000 rpm and *bmep*=2 bar. In

341   particular, the double-pilot injection strategy offers the best potentiality to reduce *CN*, *HC* and *CO* with limited

342   penalties on soot emissions. The *ppM* strategy can also lead to an improvement in the startability of a cold engine,

343   which is a typical problem for low-compression ratio engines. In fact, the longer ignition delay and poorer vaporization

344   of the fuel can inhibit fuel ignition, but double-pilot injections are able to contrast this tendency.

345   ## 5.   MEDIUM-LOAD CONDITIONS.

346   Figures 25 and 26 report the *HRR* and x_b time histories, calculated at *bmep*= 5 bar and *n*= 2000 rpm for the calibration

347   baseline points of the *pM* and *ppM* strategies, respectively. The *pM* strategy in Fig. 25 does not feature any cool flames

348   because the in-cylinder pressure and the temperature values at the pilot injection timing are more elevated than in the

349   *bmep*= 2 bar and *n*= 1500 rpm case. Instead, cool flames are present in the *HRR* diagram pertaining to the *ppM* strategy,

350   due to the early injection timing of the pilot 2 shot. The pilot combustion in the *pM* strategy (cf. the solid line with

351   triangle symbols close to $\theta \approx 355°$ *CA* in Fig. 25) is more vigorous than in the *ppM* strategy (cf. the solid line with circle

352   symbols close to $\theta \approx 358°$ *CA* in Fig. 25), due to the presence, in the former case, of a clear single-stage ignition. On the

353   other hand, since the single-stage ignition delay of the main injected fuel is longer in the *ppM* strategy, the premixed

354   combustion peak at $\theta \approx 373°$ *CA* is higher than in the *pM* case. An appreciable mixing-controlled phase is also present at

355   the end of combustion in both the *pM* and the *ppM* strategies.

356   Figures 27 and 28 show that the *bsfc* and *CN* have almost the same levels at *bmep*= 5 bar and *n*= 2000 rpm for the two

357   strategies. *HC* (Fig. 29) and *CO* (Fig. 30) become worse for *ppM*, mainly due to the longer autoignition delay, but it

358   should be pointed out that these emissions are not a reason for concern at the considered engine working condition.

359   Figure 31 shows that the NO_x-X_{EGR} dependence is the same for the two strategies. An appreciable improvement in the

360   NO_x emissions can be observed in Fig. 32 (these data have been obtained from the three-zone model) for the baseline

361   calibration point when passing from the *pM* strategy to the *ppM* one. The differences in the NO_x emissions between the

362   two calibration baseline points could be the result of the different ϕ distributions in the combustion zone, because the

363   peak T_b values and the residence times at higher temperatures than 1900 K are similar for the two calibrations (cf. Fig.

364   33). Furthermore, the higher premixing degree of the pilot injected fuel for the *pM* injection case makes the NO_x

365   emissions increase significantly in the 350° *CA*≤θ≤370° *CA* range, compared to the *ppM* strategy.

366   A slight deterioration in the soot-NO_x *EGR* trade-off can observed in Fig. 34 for the *ppM* calibration, even though the

367   maximum soot values in Figs. 34 are not critical, when a diesel particulate filter is mounted. In general, the increased

368   soot emissions represent a penalty for the considered *ppM* strategy for medium load and speed conditions (the soot

369   values in Fig. 34 are much higher than in Fig. 18). Any diminution in the ignition delay, for conventional diesel

370   combustion, causes an increase in soot emissions, and the addition of the pilot 1 injection contributes to the reduction of

371   the fuel ignition delay [4]. The liquid fuel injected during the pilot 1 shot and during most of the main injection burns in

372   the presence of combustion flames for the *ppM* strategy, and this interference between the liquid jet and the fire is a

373   remarkable source of soot (cf. Fig. 35), which cannot be balanced by the soot oxidation that occurs during the expansion

374   stroke, owing to the high temperatures induced by the retarded combustion (cf. Fig. 36). From this point of view, the

375   oxidation capability of the soot reduces in the *ppM* case, during the first part of the expansion stroke, since T_b is slightly

376   lower than in the *pM* case (Figs. 33), but increases in the exhaust manifold, because T_{exh} is significantly higher in the

377   *ppM* strategy (Fig. 36), due to the significant diffusive combustion shown in Fig. 25.

378   **6.   CONCLUSIONS.**

379   Pilot-pilot-main injection strategies have been compared with pilot-main injection strategies in a low-compression ratio

380   Euro 5 diesel engine in order to evaluate the possible benefits in engine-out emissions, combustion noise and fuel

381   consumption.

382   The considered pilot-main injection represents the state-of-the art double injection strategy for the considered engine

383   technology, whereas the parameters of the triple injection strategies have been optimized by means of a *DoE* procedure.

384   This innovative approach has allowed an effective assessment of the double pilot injection strategy in partial *PCCI*-like

385   engine working conditions to be made, since optimized double- and triple-injection engine calibrations have been

386   compared. *EGR* trade-offs have been performed in the neighborhood of the baseline points that refer to both the original

387   double-injection calibration and the triple-injection calibration optimized with the *DoE*.

388   The research investigation has been performed on the basis of experimental tests that were conducted on the engine,

389   fueled with conventional diesel fuel, in a dynamometer cell. The tests have been carried out at different steady-state

390   key-points that are representative of engine application in a vehicle over the new European driving cycle for passenger

391   cars. The experimental analysis has been supported by numerical results that were derived from the application of

392   diagnostic combustion models to the in-cylinder pressure time history. The main conclusions of the present work are

393   outlined in a synoptic way as follows.

394   •   The application of *EGR* rates close to 50% and of retarded main injection timings allows the NO_x and the soot

395   emissions to be decreased simultaneously in late *PCCI* double-injection strategies, due to an intensified fuel premixing

396   and to a reduced peak combustion temperature. The main drawbacks of these strategies at low loads are the elevated

397   combustion noise, which is due to the highly premixed combustion, and the high *HC* and *CO* engine-out emissions. The

398   high *HC* levels at the engine exhaust are generated because of the presence of overmixing regions and wall quenching

399   phenomena, whereas the high *CO* engine-out emissions are produced by the relatively low in-cylinder temperature and

400   long fuel ignition delay. Furthermore, the engine *bsfc* deteriorates, compared to the double injection strategies

401   implemented in conventional diesel engines, due to the retarded main injection timing and the reduced engine

402   compression ratio.

403   •   The employment of pilot-pilot-main injection strategies at light loads and low speeds induces an increase in the

404   time-averaged value of p_{cyl}, compared to the *pM* injection schedule, but the *HHR* combustion peaks reduce, due to the

405   fuel ignition delay diminution. The *ppM* pattern, when applied to a late *PCCI* injection strategy, leads to an increase in

406   the local fuel concentration, with respect to time and space. The generation of a suitable fuel vapor stratification, close

407   to the nozzle, reduces the impact of fuel overmixing and wall quenching and thus decreases the *HC* and *CO* engine-out

408   emissions. Significant reductions in the combustion noise, of up to 4dB, can be obtained, compared to the double

409   injection schedule. The changes in the *CN* tonality, as the *EGR* rate varies, are more pronounced for the *pM* strategy

410   than for the *ppM* one and this leads, in the latter case, to a less irritating perception of the combustion noise when the

411   *EGR* rate is modified. Finally, slight improvements in the *bsfc*-NO_x *EGR* trade-off can be observed for the case of the

412   *ppM* injection schedule.

413   •   At medium engine loads and speeds, the late *PCCI* pilot-pilot-main strategy optimized with the *DoE* allows the

414   NO_x engine-out emissions to be decreased significantly, compared to the baseline point of the *pM* injection calibration.

415   However, the NO_x-soot trade-off curve of the *pM* strategy is not improved and soot penalties are therefore incurred for

416   the *ppM* baseline calibration point, even though they are acceptable when a diesel particulate filter is mounted. The *CN*-

417 NO_x, the $bsfc$- NO_x, the HC- NO_x and the $CO–NO_x$ EGR curves do not change appreciably when the second pilot shot is

418 added to the pM injection train.

419 • On the basis of the results of the present work, a ppM injection strategy is recommended for low loads and speeds

420 to improve engine-out emissions and noise in low compression ratio engines characterized by high EGR rates. On the

421 other hand, ppM strategies do not seem to lead to any significant benefits in the higher part of the $NEDC$, compared to

422 optimized pM strategies, for the considered engine typology. Nevertheless, the choice of the most efficient calibration

423 for an engine depends to a great extent on the coupling of the combustion system to the aftertreatment devices that are

424 installed on the engine. Therefore, the ppM strategy could be considered for medium load and engine speeds in order to

425 minimize NO_x emissions.

426 ## 7. NOMENCLATURE.

427 $bmep$ brake mean effective pressure

428 $bsfc$ brake specific fuel consumption

429 CA crank angle degree

430 CN combustion noise

431 DT_1 dwell time between the pilot 1 and main injection shots

432 DT_1 dwell time between the pilot 2 and pilot 1 injection shots

433 ECU electronic control unit

434 EGR exhaust gas recirculation

435 HC unburned hydrocarbons

436 HRR heat release rate

437 m_a inducted air per engine cycle and per cylinder

438 $\dot{m}_a$ fresh air mass flow-rate

439 $\dot{m}_{EGR}$ exhaust gas mass flow-rate

440 $MFB50$ angle at which 50% of the combustion mixture has burned

441 n engine speed

442 NO_x nitrogen oxides

443 OEM original equipment manufacturer

444 p_{cyl} in-cylinder pressure

445 p_{rail} nominal rail pressure level

446 $PCCI$ premixed charge compression ignition

447	PM	particulate matter
448	q_{Pil1}	volume of fuel injected in the pilot 1 injection
449	q_{Pil2}	volume of fuel injected in the pilot 2 injection
450	SOI_{Main}	electrical start of the main injection
451	SOI_{Pil}	electrical start of the pilot injection
452	Sw	swirl actuator position
453	T_b	burned gas temperature
454	TDC	top dead center
455	X_{EGR}	mass fraction of exhaust gas recirculation
456	ϕ	equivalence ratio
457	λ	relative air-to-fuel ratio
458	θ	crankshaft angle in the simulations

459 **8. REFERENCES.**

460 [1] Heywood, J. B., 1988, "Internal combustion engine fundamentals", McGraw Hill, New York.

461 [2] Maiboom, A., Tauzia, X., and Hetet, J. F., 2008, "Experimental study of various effects of exhaust gas

462 recirculation on combustion and emissions of an automotive direct injection diesel engine", *Energy*, 33,

463 pp. 22-34.

464 [3] Ehleskog, R., Ochoterena, R. L., and Andersson., S., 2007, "Effects of multiple injections on engine-out

465 emission levels including particulate mass from an HSDI diesel engine", SAE paper. 2007-01-0910.

466 [4] Suh, K. H., 2014, "Study on the twin-pilot-injection strategies for the reduction in the exhaust emissions

467 in a ow-compression engine", *Proc. IMechE Part D: J. of Automobile Engineering*, vol. 228(3), pp. 335-343.

468 [5] Lee, J. W., Choi, S. M., Yu, S., Choi, H., and Min, K. D., 2013, "Comparison of the effects of multiple

469 injection strategy on the emissions between moderate and heavy EGR rate conditions: part 1-pilot

470 injections", *Journal of Mechanical Science and Technology*, 27(4), pp. 1135-1141.

471 [6] Tullis, S., and Greeves, G., 1996, " Improving NO_x versus bsfc with EUI 200 using EGR and pilot

472 injection for heavy duty diesel engines", SAE paper No. 960843.

473   [7] Bhatt, N. M., Rathod, P. P., Sorathiya, A. S., and Patel, R., 2013, "Effect of the multiple injection on the

474   performance and emission of diesel engine. A review study", *International Journal of Emerging Technology*

475   *and Advanced Technology*, vol. 3 (3).

476   [8] Busch, S., Zha, K. and Miles, P.C., 2014, "Investigations of closely coupled pilot and main injections as a

477   mean to reduce combustion noise", 8th Thiesel Conference, Valencia 9th-12th September.

478   [9] Han, Z., Uludogan, A., Hampson, G. J., and Reitz, R. D., 1996, "Mechanism of soot and NO_x emission

479   reduction using multiple-injection in diesel engine", SAE paper 960633.

480   [10] Yun, H. H., Sellnau, M., Milovanovic, N., and Zuelch, S., 2008, "Development of premixed low-

481   temperature diesel combustion in a HSDI engine", SAE paper no. 2008-01-0639.

482   [11] Helmantel, A., and Golovitchev, 2009, "Injection strategy optimization for a light duty DI diesel engine

483   in medium load conditions with high EGR rates", SAE paper no. 2009-01-1441.

484   [12] Nishimura, T., Satoh, K., Takahashi, S., and Yokota, K., 1998, "Effects of fuel injection rate on

485   combustion and emission in a DI diesel engine", SAE paper 981929.

486   [13] DieselNet, Engine and emission technology online, since 1997, www.dieselnet.com.

487   [14] Kastner, O., Atzler, F., Juvenelle, C., Rotondi, R., and Weigand, A., 2009, "Directly actuated piezo

488   injector for advanced injection strategies towards cleaner diesel engines" Towards Clean Diesel Engines,

489   TCDE 2009.

490   [15] Predelli, O., Gratzke, R., Sommer, A., Marohn, R., Atzler, F., Schule, H., Kastner, O., and Nozeran, N.,

491   2010, "Continuous injection-rate shaping for passenger-car diesel engines – Potential, limits and feasibility",

492   31st International Vienna Engine Symposium.

493   [16] Payri, F., Broatch, A., Salavert, J. M., Martín, J.,

494   2010, "Investigation of Diesel combustion using multiple injection strategies for idling after cold start of

495   passenger-car engines", *Experimental Thermal and Fluid Science*, 34, pp. 857–865.

496   [17] Tow, T. C., Pierpont, D. A., and Reitz, R. D., 1994, "Reducing Particulate and NO_x emissions by using

497   multiple injections in a heavy duty D.I. diesel engine", SAE paper 940897.

498   [18] Hotta, Y., Inayoshi, M., Nakakita, K., Fujiwara, K., and Sakata, I., 2005, " Achieving lower exhaust

499   emissions and better performance in an HSDI diesel engine with multiple injection", SAE paper no. 2005-

500   01-0928.

501   [19] Badami, M., Mallamo, F., Millo, F., and Rossi, E. E., 2003, "Experimental investigation on the effect of

502   multiple injection strategies on emissions, noise and brake specific fuel consumption of an automotive direct

503   injection common-rail diesel engine", *International journal of engine research* 4(4), pp. 299-314.

504   [20] Okude, K., Mori, K., Shiino, S., Yamada, K., and Matsumoto, Y., 2007, "Effects of multiple injections

505   on diesel emission and combustion characteristics", SAE paper. No. 2007-01-4178.

506   [21] Mobasheri, R. Peng, Z., 2012, "Investigation of pilot and multiple injection parameters on mixture

507   formation and combustion characteristics in a heavy duty DI-diesel engine", SAE paper 2012-04-16.

508   [22] Schoppe, D., Zulch, S., Harfy, M., Geurts, D., Jaorach, R. W., and Baker, N., ,2008, "Delphi Common

509   rail system with direct acting injector", MTZ 10/2008, vol. 69, pp. 32-38.

510   [23] Ricaud, J.C., and Lavoisier, F., 2004, "Optimizing the multipleinjection settings on an HSDI diesel

511   engine" Conference on Thermo- and fluid-dynamics processes in diesel Engines, Valencia, Spain, 11–13

512   September 2002

513   [24] Zheng Z, Yue L, Liu H, Zhu Y, Zhong X, Yao M, 2015, "Effect of two-stage injection on combustion

514   and emissions under high EGR rate on a diesel engine by fueling blends of diesel/gasoline, diesel/n-butanol,

515   diesel/gasoline/n-butanol and pure diesel", *Energy Conversion and Management*, 90, pp. 1-15.

516   [25] d'Ambrosio, S., Finesso, R., and Spessa, E., 2011, "Calculation of Mass Emissions, Oxygen Mass

517   Fraction And Thermal Capacity Of The Inducted Charge In SI And Diesel Engines From Exhaust And

518   Intake Gas Analysis", *Fuel*, n. 90, issue 1, pp. 152-166.

519   [26] Finesso, R., and Spessa, E, 2014, "A real time zero-dimensional diagnostic model for the calculation of

520   in-cylinder temperatures, HRR and nitrogen oxides in diesel engines. Energy Conversion and Management

521   79 498–510. http://dx.doi.org/10.1016/j.enconman.2013.12.045.

[27] Baratta M., Catania A.E., Ferrari A., Finesso R. and Spessa E., 2011, "Premixed-Diffusive Multizone Model for Combustion Diagnostics in Conventional and PCCI Diesel Engines", *ASME Trans*. *Journal of Engineering for Gas Turbines and Power*, vol. 133 n. 10, Art. No. 102801, pp. 1-13.

[28] Fang C, Yang F, Ouyang M, Gao G, Chen L, 2013, "Combustion mode switching control in a HCCI diesel engine, *Applied Energy* 110 (2013) 190–200", http://dx.doi.org/10.1016/j.apenergy.2013.04.060.

[29] Agarwal D, Singh SK, Agarwal AK, 2011, "Effect of exhaust gas recirculation (EGR) on performance, emissions, deposits and durability of a constant speed compression ignition engine". *Applied Energy* 2011;88(8):2900–7.

[30] Kiplimo, R., Tomita, E., Kawahara, N., and Yokobe, S., 2012, "Effects of spray impingement, injection parameters and *EGR* on the combustion and emission characteristics of a PCCI diesel engine", *Applied Thermal Engineering*, vol. 37, pp. 165-175.

[31] Mendez, S., and Thirouard, B., 2008, "Using multiple injection strategies in diesel combustion: potential to improve emissions, noise and fuel economy trade-off in low CR engine", SAE paper 2008-01-1329.

[32] Broath, A., Ruiz, S., Margot, X., and Gil, A., 2010, "Methodology to estimate the threshold in-cylinder temperature for self-ignition of fuel during cold start of diesel engines", *Energy*, 35, pp. 2251-2560

[33] McMillan, D., La Rocca, A., Shayler, P. J., et al., 2008, "The effect of reducing compression ratio on the work output and heat release characteristics of a DI diesel under cold start conditions", SAE Paper No. 2008-01-1306.

[34] Kiplimo R, Tomita, Kawahara N, Yokobe S, 2012, "Effects of spray impingement, injection parameters, and EGR on the combustion and emission characteristics of a PCCI diesel engine", *Applied Thermal Engineering* 37 (2012) 165-175. doi:10.1016/j.applthermaleng.2011.11.011.

[35] Saxena S, Dedoya ID, 2013, "Fundamental phenomena affecting low temperature combustion and HCCI engines, high load limits and strategies for extending these limits, *Progress in Energy and Combustion Science* 39 (2013) 457-488. http://dx.doi.org/10.1016/j.pecs.2013.05.002.

546 [36] Suh HK, Investigations of multiple injection strategies for the improvement of combustion and exhaust

547 emissions characteristics in a low compression ratio (CR) engine, 2011, *Applied Energy* 88 (2011) 5013–

548 5019. doi:10.1016/j.apenergy.2011.06.048.

549 [37] Dec, J., and Canaan, R. E., 1998 "PLIF imaging of NO formation in a DI diesel engine", *SAE*

550 *Transactions*, 107, No. 3, pp. 176-204.

551 [38] Akihama, K., Takatori, Y., Inagaki, K., Sakaki, S., and Dean, A. M., 2001, "Mechanism of smokeless

552 rich diesel combustion by reducing temperature", SAE paper no. 2001-01-0655.

553 **9. TABLES AND FIGURES**

554

Engine type	2.0L Euro 5
Displacement	1956 cm^3
Bore × stroke	83.0 mm × 90.4 mm
Compression ratio	16.3
Valves per cylinder	4
Turbocharger	Twin-stage with valve actuators and WG
Fuel injection system	Common Rail 2000 bar piezo
Specific power and torque	71 kW/l – 205 Nm/l
EGR system type	Short-route cooled EGR
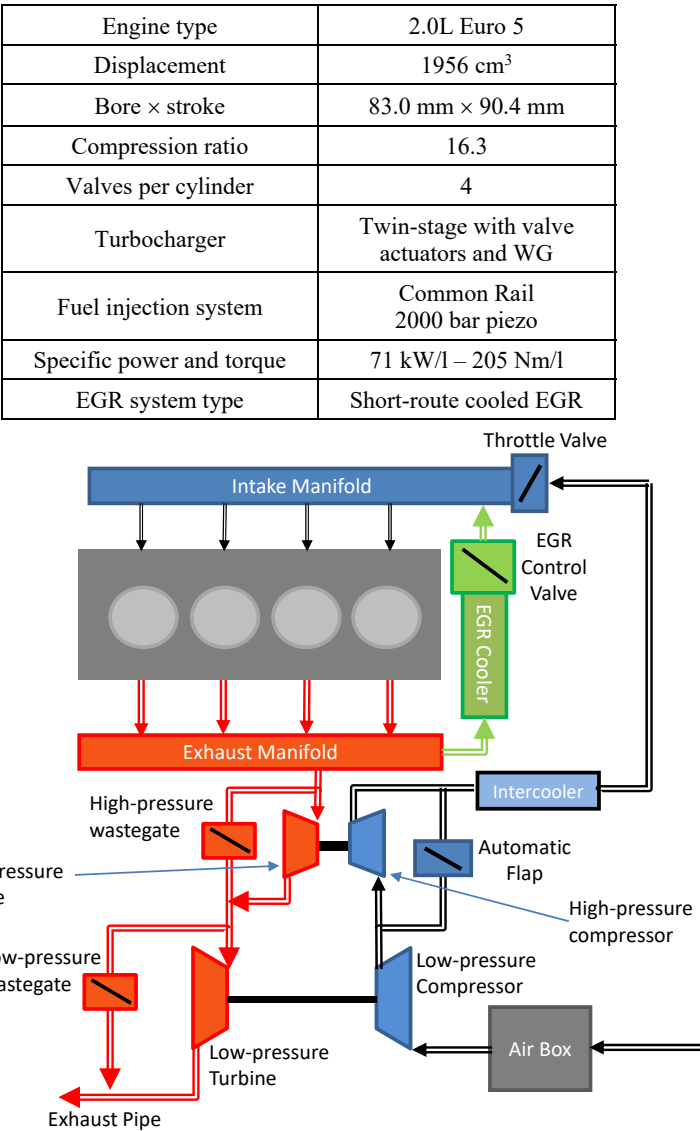
Table 1. Main specifications and schematic of the tested engine.

Quantity	Levels	Optimization
SOI_{Main} [°CA bTDC]	−4.5 −2.88 −1.25 0.37 2	−0.2
m_a [mm³/(stk·cyl)]	230 245 260	230
Sw [%]	30 38.8 47.5 56.3 65	39.7
p_{Rail} [bar]	300 450 600	516.6
q_{Pil1} [mm³/(stk·cyl)]	0.8 1.23 1.65 2.08 2.5	1
DT_1 [μs]	300 625 950 1275 1600	446
q_{Pil2} [mm³/(stk·cyl)]	0.8 1.1 1.4 1.7 2	2
DT_2 [μs]	300 625 950 1275 1600	907

Table 2: Levels considered in the variation list and optimized values of the input variables for the triple injection at 1500×2.

555
556

Quantity	Levels	Optimization
SOI_{Main} [°CA bTDC]	−1 1 3	1
m_a [mm³/(stk·cyl)]	360 380 390 400 420	362.2
Sw [%]	30 38.8 47.5 56.3 65	35.5
p_{Rail} [bar]	750 833.3 950 1016.7 1150	826.4
q_{Pil1} [mm³/(stk·cyl)]	0.8 1.23 1.65 2.08 2.5	0.8
DT_1 [µs]	300 625 950 1275 1600	773
q_{Pil1} [mm³/(stk·cyl)]	0.8 1.1 1.4 1.7 2	0.8
DT_2 [µs]	600 850 1100 1350 1600	1600

Table 3: Levels considered in the variation list and optimized values of the input variables for the triple injection at 2000×5.

557

Strategy	NOx [g/kWh]	HC [g/kWh]	CO [g/kWh]	Soot [g/kWh]	bsfc [g/kWh]	CN [dBA]
pM	0.53	2	8.8	0.04	299	76.7
ppM	min	≤ 2	≤ 9	≤ 0.3	≤ 305	≤ 74

Table 4: Reference values of the reference *pM* calibration baseline point and constraints for the optimization of the *ppM* injection strategy at 1500×2.

558

Strategy	NO$_x$ [g/kWh]	HC [g/kWh]	CO [g/kWh]	Soot [g/kWh]	bsfc [g/kWh]	CN [dBA]
pM	0.99	0.3	1.9	0.3	248	86.5
ppM	min	≤0.5	≤5	≤1.2	≤255	≤86.5

Table 5. Reference values of the reference *pM* calibration baseline point and constraints for the optimization of the *ppM* injection strategy at 2000×5.

559
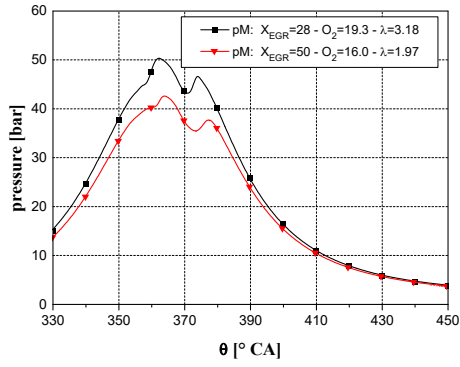
Figure 1. *p_cyl* versus θ distribution for X_{EGR}=28% and X_{EGR}=50% (*bmep*=2 bar, *n*=1500 rpm).
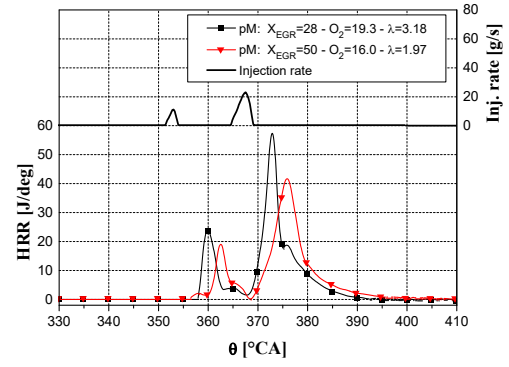
Figure 2. *HRR* versus θ distribution for X_{EGR}=28% and X_{EGR}=50% (*bmep*=2 bar, *n*=1500 rpm).
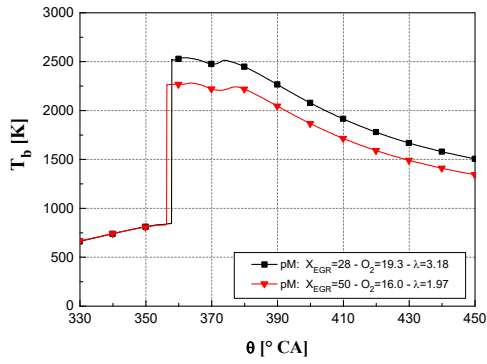
Figure 3. *T_b* versus θ distribution for X_{EGR}=28% and X_{EGR}=50% (*bmep*=2 bar, *n*=1500 rpm).
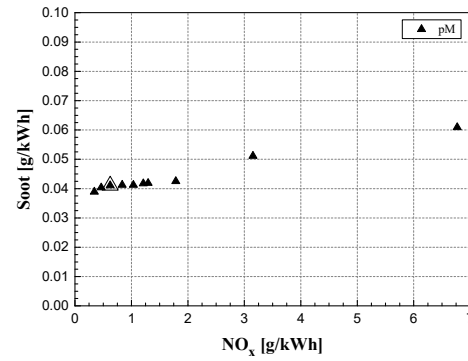
Figure 4. Soot- *NO_x* for different X_{EGR} values (*bmep*=2 bar, *n*=1500 rpm).
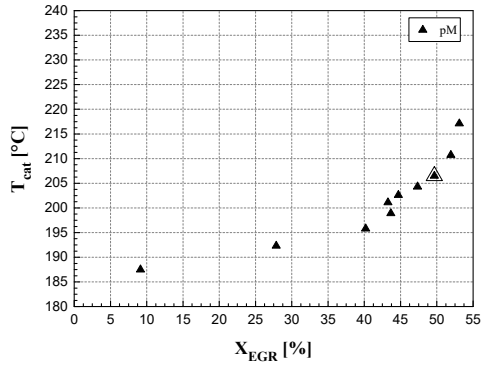
Figure 5. Gas temperature *T_cat* as a function of X_{EGR} (*bmep*=2 bar, *n*=1500 rpm).
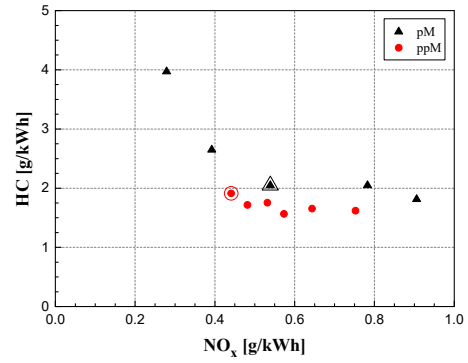
Figure 6. *HC-NO_x* trade-off for the *pM* and *ppM* strategies (*bmep*=2 bar, *n*=1500 rpm).
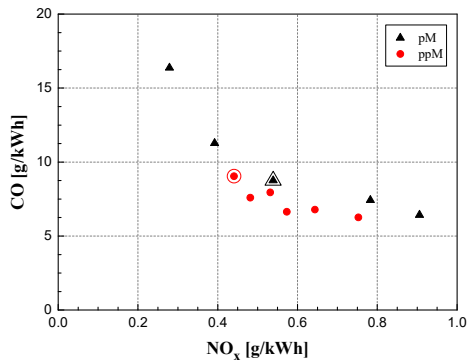
Figure 7. *CO-NO_x* trade-off for the *pM* and *ppM* strategies (*bmep*=2 bar, *n*=1500 rpm).
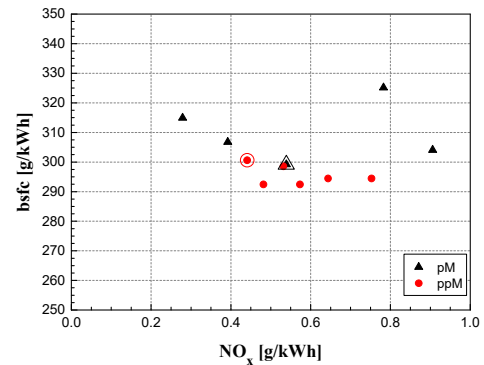
Figure 8. *bsfc-NO_x* trade-off for the *pM* and *ppM* strategies (*bmep*=2 bar, *n*=1500 rpm).

560
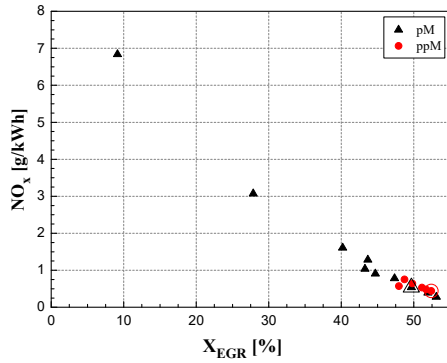
Figure 9. *NO$_X$* versus *X$_{EGR}$* for the *pM* and *ppM* strategies (*bmep*=2 bar, *n*=1500 rpm).
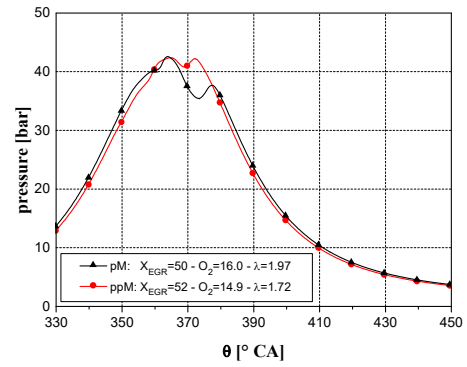
Figure 10. *p$_{cyl}$* versus θ distribution for *pM* and *ppM* strategies (*bmep*=2 bar, *n*=1500 rpm).
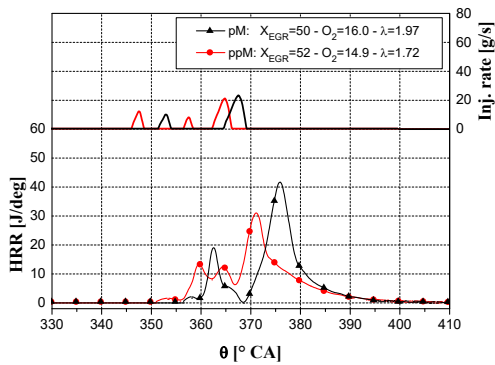
Figure 11. HRR versus θ distribution for the pM and ppM strategies (bmep=2 bar, n=1500 rpm)
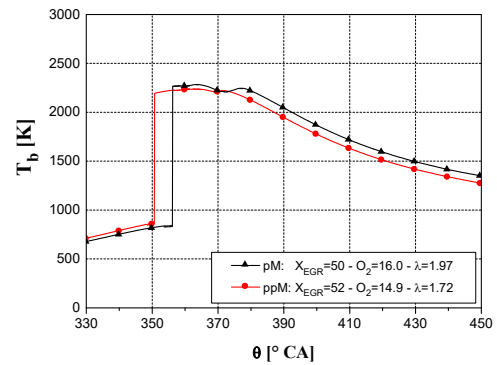
Figure 12. *T$_b$* versus θ distribution for *pM* and *ppM* strategies (*bmep*=2 bar, *n*=1500 rpm).
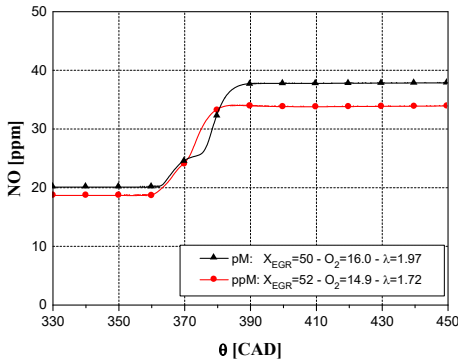
Figure 13. *NO* versus θ distribution for *pM* and *ppM* strategies (*bmep*=2 bar, *n*=1500 rpm).
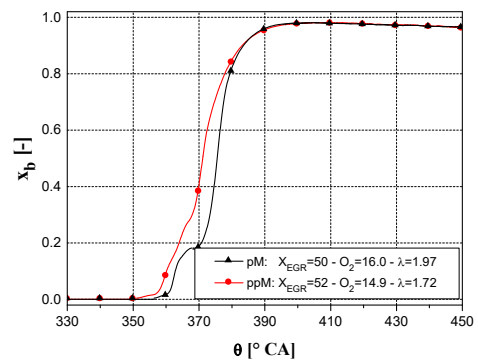
Figure 14. *x$_b$* versus θ distribution for *pM* and *ppM* strategies (*bmep*=2 bar, *n*=1500 rpm).
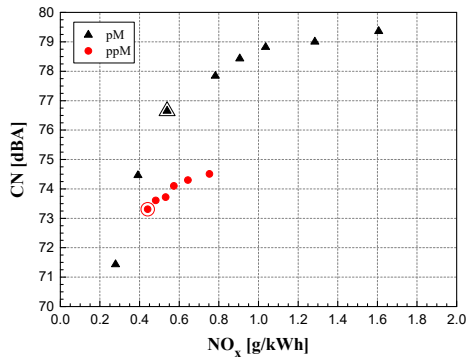
Figure 15. *CN-NO$_X$* trade-off for the *pM* and *ppM* strategies (*bmep*=2 bar, *n*=1500 rpm).
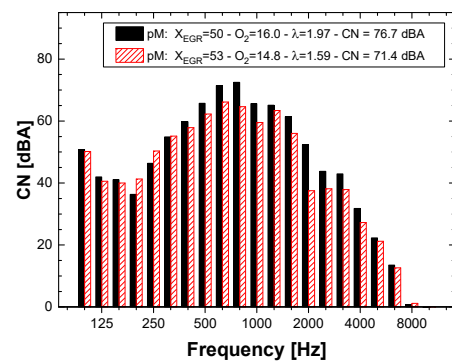
Figure 16. One-third octave frequency bands of *CN* for the *pM* strategy (*bmep*=2 bar, *n*=1500 rpm).

561
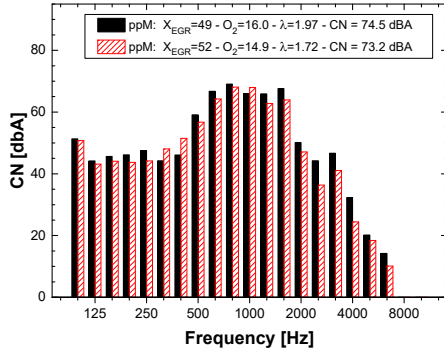
Figure 17. One-third octave frequency bands of *CN* for the *ppM* strategy (*bmep*=2 bar, *n*=1500 rpm).
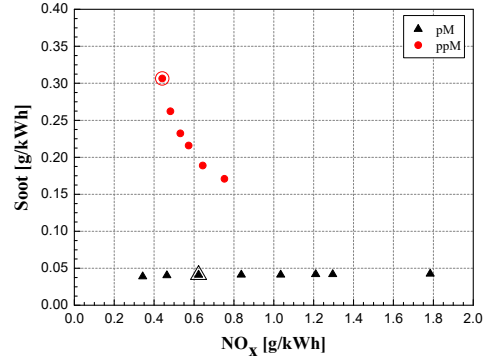
Figure 18. Soot-*NO$_X$* trade-off for the *ppM* strategy (*bmep*=2 bar, *n*=1500 rpm).
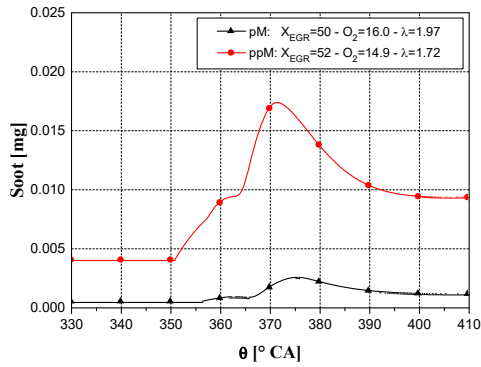
Figure 19. *PM* versus θ distribution for *pM* and *ppM* strategies (*bmep*=2 bar, *n*=1500 rpm).
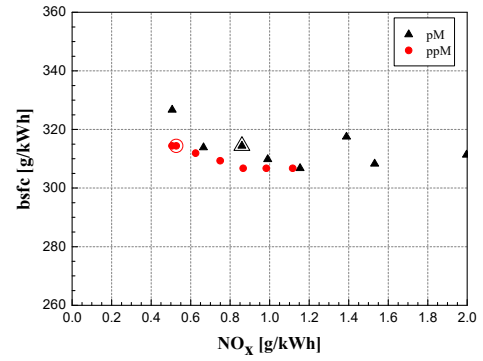
Figure 20. *bsfc-NO$_X$* trade-off for the *pM* and *ppM* strategies (*bmep*=2 bar, *n*=2000 rpm).
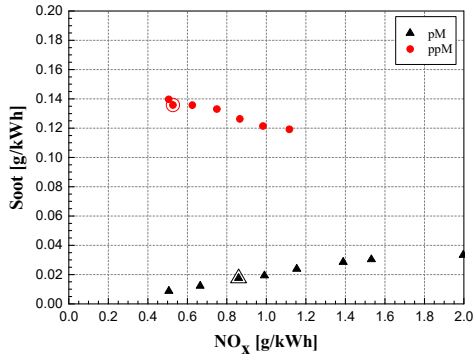
Figure 21. Soot-*NO$_X$* trade-off for the *pM* and *ppM* strategies (*bmep*=2 bar, *n*=2000 rpm).
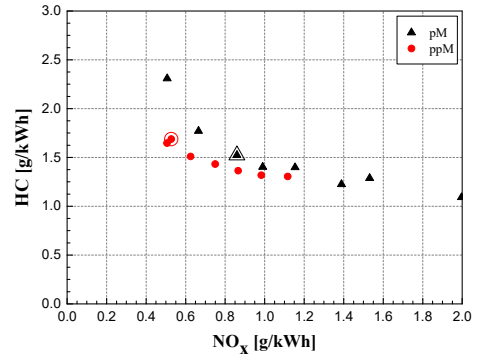
Figure 22. HC-*NO$_X$* trade-off for the *pM* and *ppM* strategies (*bmep*=2 bar, *n*=2000 rpm).
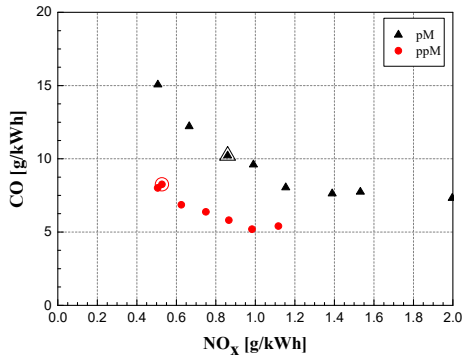
Figure 23. *CO-NO$_X$* trade-off for the *pM* and *ppM* strategies (*bmep*=2 bar, *n*=2000 rpm).
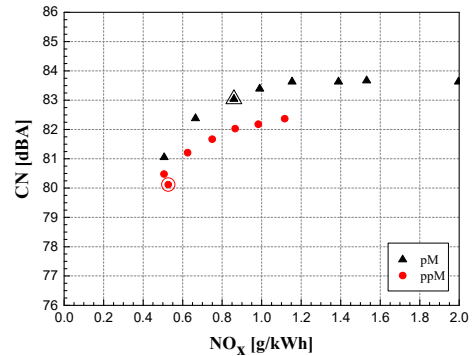
Figure 24. *CN-NO$_X$* trade-off for the *pM* and *ppM* strategies (*bmep*=2 bar, *n*=2000 rpm).
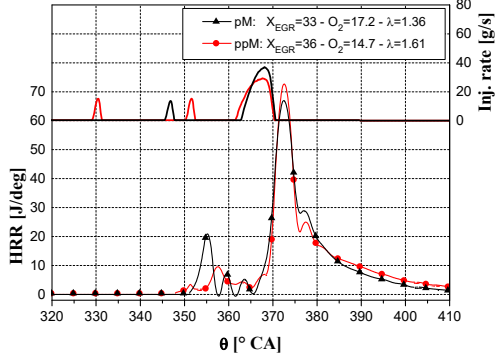
Figure 25. *HRR* versus θ distribution for the *pM* and *ppM* strategies (*bmep*=5 bar, *n*=2000 rpm).
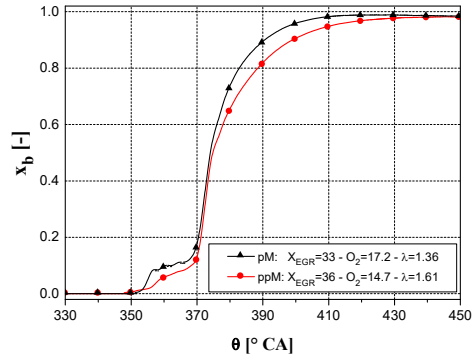
Figure 26. x_b versus θ distribution for *pM* and *ppM* strategies (*bmep*=5 bar, *n*=2000 rpm).
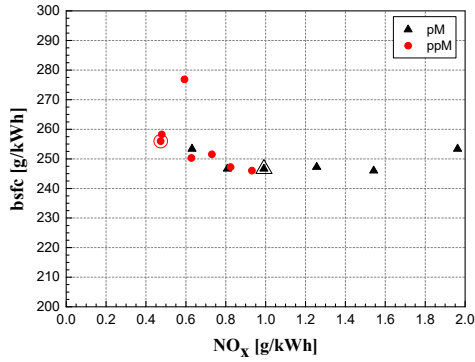
Figure 27. *bsfc-NO_X* trade-off for the *pM* and *ppM* strategies (*bmep*=5 bar, *n*=2000 rpm).
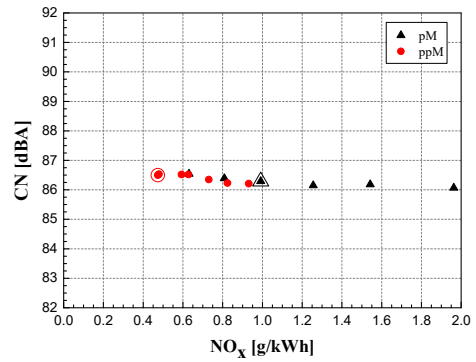
Figure 28. *CN-NO_X* trade-off for the *pM* and *ppM* strategies (*bmep*=5 bar, *n*=2000 rpm).
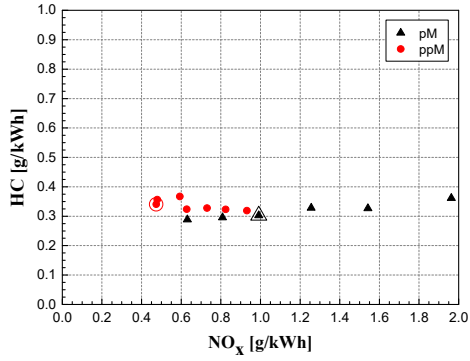
Figure 29. *HC-NO_X* trade-off for the *pM* and *ppM* strategies (*bmep*=5 bar, *n*=2000 rpm).
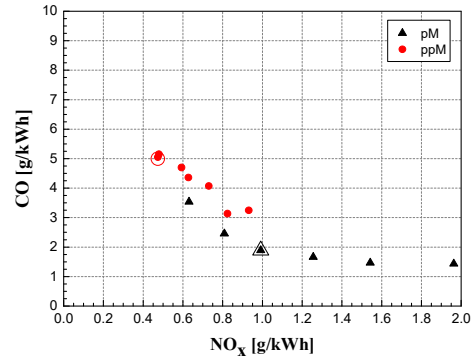
Figure 30. *CO-NO_X* trade-off for the *pM* and *ppM* strategies (*bmep*=5 bar, *n*=2000 rpm).
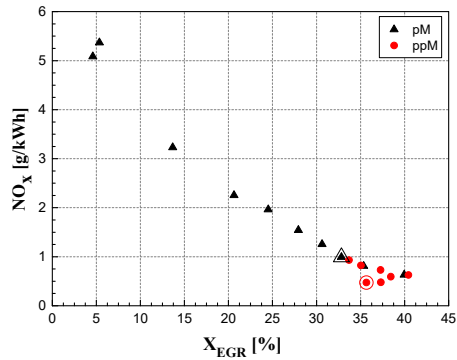
Figure 31. *NO_x* versus X_{EGR} for the *pM* and *ppM* strategies (*bmep*=5 bar, *n*=2000 rpm).
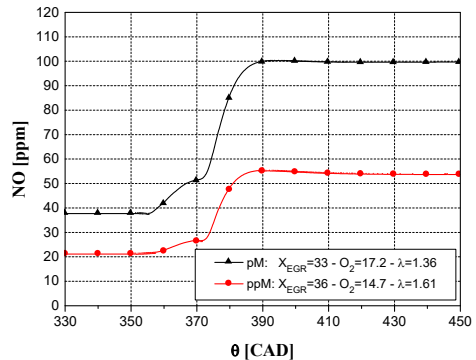
Figure 32. *NO_x* versus θ distribution for the *pM* and *ppM* strategies (*bmep*=5 bar, *n*=2000 rpm).
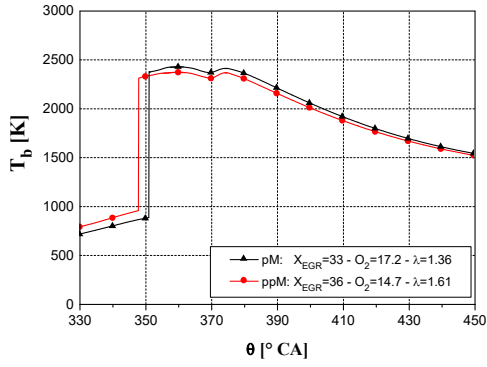
Figure 33. T_b versus θ distribution for *pM* and *ppM* strategies (*bmep*=5 bar, *n*=2000 rpm).
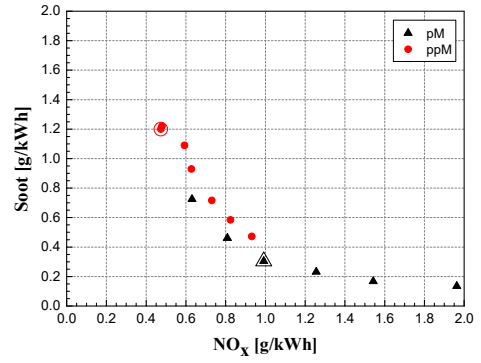
Figure 34. Soot-NO_X trade-off for the *pM* and *ppM* strategies (*bmep*=5 bar, *n*=2000 rpm).
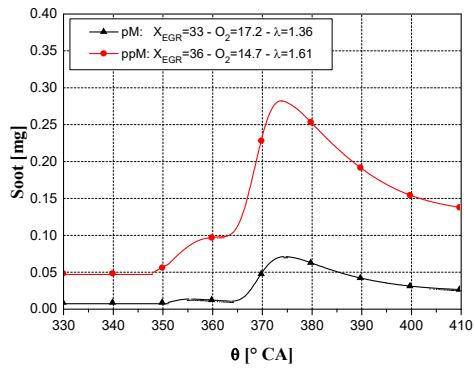

Figure 35. Soot versus θ distribution for the *pM* and *ppM* strategies (*bmep*=5 bar, *n*=2000 rpm).
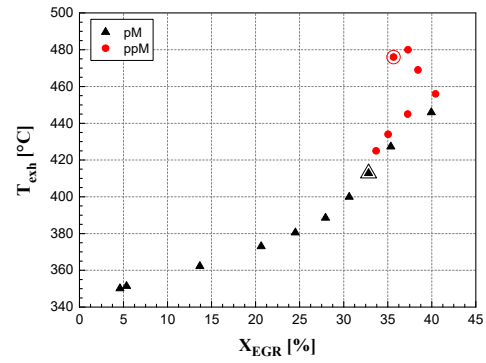

Figure 36. T_{exh} versus X_{EGR} for the *pM* and *ppM* strategies (*bmep*=5 bar, *n*=2000 rpm).